nanomaterials

MDPI

Article

Temperature-Program Assisted Synthesis of Novel Z-Scheme $CuBi_2O_4/\beta$-Bi_2O_3 Composite with Enhanced Visible Light Photocatalytic Performance

Xiaojuan Chen [1], Ning Li [2,*], Runliang Zhu [3,4], Shuai Li [1], Chunmo Yu [1], Wei Xia [1], Song Xu [1] and Xin Chen [1]

1 School of Environment and Chemical Engineering, Foshan University, Foshan 528000, China; xjchen0218@163.com (X.C.); fky0322017@126.com (S.L.); cym0171@126.com (C.Y.); lining159.com@163.com (W.X.); xusong018@163.com (S.X.); fschenxin@163.com (X.C.)
2 School of Marine Sciences, Sun Yat-sen University, Guangzhou 510275, China
3 Guangdong Provincial Key Laboratory of Mineral Physics and Materials, Guangzhou Institute of Geochemistry, Guangzhou 510640, China; zhurl@gig.ac.cn
4 CAS Key Laboratory of Mineralogy and Metallogeny, Guangzhou Institute of Geochemistry, Chinese Academy of Sciences, Guangzhou 510640, China
* Correspondence: lining43@mail.sysu.edu.cn; Tel.: +86-757-8278-7103

Received: 25 June 2018; Accepted: 26 July 2018; Published: 28 July 2018

Abstract: Novel Z-Scheme $CuBi_2O_4/\beta$-Bi_2O_3 composite photocatalysts with different mass ratios and calcination temperatures were firstly synthesized by the hydrothermal method following a temperature-programmed process. The morphology, crystal structure, and light absorption properties of the as-prepared samples were systematically characterized, and the composites exhibited enhanced photocatalytic activity toward diclofenac sodium (DS) degradation compared with $CuBi_2O_4$ and β-Bi_2O_3 under visible light irradiation. The optimal photocatalytic efficiency of the composite, achieved at the mass ratio of $CuBi_2O_4$ and β-Bi_2O_3 of 1:2.25 and the calcination temperature of 600 °C is 92.17%. After the seventh recycling of the composite, the degradation of DS can still reach 82.95%. The enhanced photocatalytic activity of $CuBi_2O_4/\beta$-Bi_2O_3 is closely related to $OH^{\bullet}$, h^+ and $O_2^{\bullet -}$, and the photocatalytic mechanism of $CuBi_2O_4/\beta$-Bi_2O_3 can be explained by the Z-Scheme theory.

Keywords: $CuBi_2O_4/\beta$-Bi_2O_3; temperature programmed; semiconductors; Z-Scheme; visible light; organics

1. Introduction

Diclofenac sodium (DS) is a very effective anti-inflammatory drug widely used in many countries [1,2]. Due to the poor absorbability of organisms to DS, most of the DS will be released into the environment after it is taken [1]. However, long-term exposure to a DS-polluted environment will cause serious risk to ecosystems and human health [3,4]. Therefore, effective degradation technologies for DS should be explored to control its persistent contamination.

Semiconductor photocatalytic technology has aroused widespread interest in organic pollution control [5–8] due to its advantages of rich catalysts, mild reaction conditions, fast reaction speed, and no secondary pollution. In past decades, titanium dioxide (TiO_2) has attracted considerable attention for its low cost and chemical inertness [8–10]. However, the large band gap of TiO_2, which is approximately 3.2 eV, limits its absorption of sunlight to the ultraviolet (UV) region [10,11]. Because the visible light occupies 43% of sunlight, whereas UV light occupies only 4%, the development of visible-light responsive semiconductor photocatalysts is becoming a research hotspot [12–15].

$CuBi_2O_4$ possesses a strong visible light response, excellent chemical stability, high conduction band position, and strong reducing ability [16–18]. However, the single $CuBi_2O_4$ exhibits poor photocatalytic performance [17]. Some related studies suggest its activity could be improved through the synergistic effect with other metal oxide semiconductors [17,19,20]. Bi_2O_3, a visible light-responsive semiconductor material, is regarded as a promising photocatalyst for organic pollutant degradation [21,22]. This is mainly due to that the energy band gap (in the range from 2.4 to 3.2) of Bi_2O_3 can be tuned by employing different synthesis techniques, such as sol gel, hydrothermal/solvothermal and solid-state decomposition methods [21,23,24]. β-Bi_2O_3, as one of the six different polymorphs of Bi_2O_3 (i.e., α-, β-, γ-, δ-, ω- and ε-polymorph), exhibits a narrower band gap with the strongest light-absorption ability than other phases [23,25–27]. Yet the photocatalytic activity of pure β-Bi_2O_3 is still far from satisfactory for the fast recombination of photogenerated charges [26,28].

In theory, $CuBi_2O_4$ coupling with β-Bi_2O_3 could form the hybrid composite via matching the band structure of each other with significantly enhanced photocatalytic activity. Nevertheless, the research on the temperature-programmed synthesis and photocatalytic application of a $CuBi_2O_4/\beta$-Bi_2O_3 system has not been investigated in detail. In this study, novel $CuBi_2O_4/\beta$-Bi_2O_3 composite photocatalysts with different mass ratios and calcination temperatures were firstly synthesized by the hydrothermal method following a temperature-programmed process. The as-synthesized composites were systematically characterized and their photocatalytic performance was carefully investigated by the degradation of DS under visible-light irradiation ($\lambda > 400$ nm). Moreover, the active species in the $CuBi_2O_4/\beta$-Bi_2O_3 photocatalytic system were discussed through the free radical capture experiments, and the photocatalytic mechanism of $CuBi_2O_4/\beta$-Bi_2O_3 was also put forward.

2. Materials and Methods

2.1. Materials

All reactants and solvents were analytical grade and used without further purification. $Bi(NO_3)_3{\cdot}5H_2O$, $Cu(NO_3)_2{\cdot}3H_2O$, Na_2CO_3, NaOH, HNO_3, gluconic acid, tert-butanol (*t*-BuOH), para-benzoquinone (BZQ), disodium ethylenediaminetetr-aacetate (Na_2-EDTA), ethanol, and diclofenac sodium were obtained from Sinopharm Chemical Reagent Co., Ltd., (Shanghai, China). Ultrapure water was used throughout this study.

2.2. Synthesis of $CuBi_2O_4/\beta$-Bi_2O_3

The detailed synthesis pathway of $CuBi_2O_4/\beta$-Bi_2O_3 is illustrated in Figure 1. Firstly, $CuBi_2O_4$ was prepared through a simple hydrothermal method, and the detailed experiment processes are similar to that reported by our previous paper [16]. Secondly, a core-shell structural $CuBi_2O_4$@C was synthesized, that is, 0.1 g of $CuBi_2O_4$ was ultrasonically dispersed into 70 mL of aqueous solution (with 0.3 mL gluconic acid), and then the solution was transferred into a 100-mL sealed Teflon-lined stainless steel autoclave for 4 h at 180 °C. When the autoclave was cooled naturally to room temperature, the precipitate was isolated by centrifugation and washed several times with distilled water. Thirdly, a temperature-programmed method was used to synthesize the $CuBi_2O_4/\beta$-Bi_2O_3. Then 0.1 g of $CuBi_2O_4$@C obtained above was ultrasonically dispersed into 20 mL HNO_3 solution (1 mol/L) to obtain solution A; 0.39 mmol $Bi(NO_3)_3{\cdot}5H_2O$ was completely dissolved into another 20 mL HNO_3 solution (1 mol/L) under the acute agitation to obtain solution B; 2.34 mmol Na_2CO_3 was dissolved into 40 mL ultrapure water to obtain solution C. After solutions A and B were well mixed, solution C was added into the mixture drop by drop, and a large amount of white precipitate was produced. Then the washed precipitate by ethanol and ultrapure water was placed into a temperature-programmed furnace, and the reaction furnace was set to be heated to 600 °C within 30 min and kept at this temperature for 5 h. The $CuBi_2O_4/\beta$-Bi_2O_3 with mass ratio of 1:2.25 at different calcination temperatures of 400 °C, 600 °C and 800 °C was obtained through changing the temperature of the reaction furnace. In addition, the $CuBi_2O_4/\beta$-Bi_2O_3 with different mass ratios of 1:1, 1:2.25 and 1:4 was obtained through adjusting

the added amount of $Bi(NO_3)_3 \cdot 5H_2O$ and Na_2CO_3. For composition, the pure $CuBi_2O_4$ and β-Bi_2O_3 were also prepared through the above synthesis process, and the detailed synthesis steps can also be seen from the Figure 1.

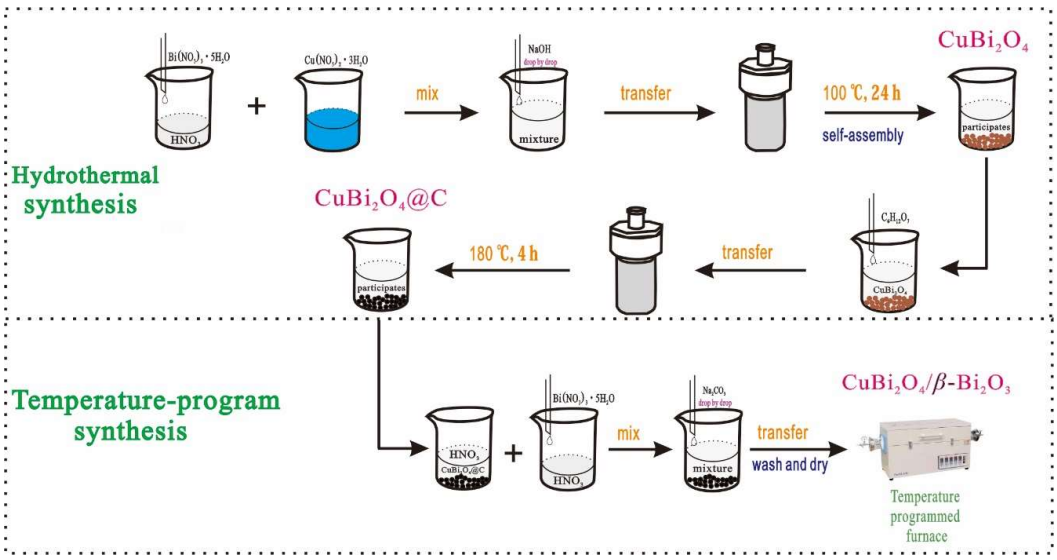

Figure 1. The detailed synthesis pathway of $CuBi_2O_4/\beta$-Bi_2O_3.

2.3. Characterization

Powder X-ray diffraction (XRD) patterns were examined to study the crystal structure and phase composition of the materials using the D/max 2500 PC (Rigaku, Japan) instrument with Cu Kα radiation (40 kV, 100 mA) at a rate of 4.0°/min over a 2θ range of 20°–60°. Morphologies of the samples were characterized by scanning electron microscopy (SEM, JSM-6360LV, JEOL, Tokyo, Japan). Ultraviolet-visible (UV-Vis) diffusive reflectance spectra were obtained by a Shimadzu UV-2550 spectrophotometer (Shimadzu, Kyoto, Japan) over the analysis range from 200 to 800 nm. X-ray photoelectron spectra (XPS) were recorded using the ESCALAB 250 instrument (Thermo Scientific, Waltham, MA, USA) with Al Kα radiation.

2.4. Photocatalytic Performance Experiments

The photocatalytic performance experiments were conducted in photoreaction apparatus (BL-GHX-V, Bilang Biological Science and Technology Co., Ltd., Xi'an, China) using a 300 W Xe lamp with an ultraviolet cutoff filter (providing visible light $\geq$ 400 nm) as the light source. In each experiment, a 25 mg photocatalyst was added to 50 mL of DS solution (8 mg/L). Before irradiation, the solution was magnetically stirred in the dark for 30 min to reach the adsorption-desorption equilibrium. As the reaction time elapsed, the sample was taken out and filtered immediately with 0.45 μm membrane filters, the concentrations of DS and Total Organic Carbon (TOC) are measured by a high performance liquid chromatography (HPLC, Agilent 1260, Santa Clara, CA, USA) and TOC (Shimadzu TOC-V_{CPH}, Kyoto, Japan) analyzer, respectively. In addition, repeated experiments for DS degradation were also conducted to study the stability of the as-prepared photocatalysts, and the operation processes were similar to the photocatalytic experiments. All experiments were repeated twice and the data shown in the article was averaged.

2.5. Analysis of Reactive Species

Free radical capture experiments were used to ascertain the reactive species of $CuBi_2O_4/\beta$-Bi_2O_3 photocatalytic system, and tert-butanol (*t*-BuOH) was chosen as the hydroxyl radical ($OH^{\bullet}$)

scavenger, disodium ethylenediamine tetraacetate (EDTA-Na_2) was chosen as the hole (h^+) scavenger, benzoquinone (BZQ) was chosen as the superoxide radical ($O_2^{\bullet-}$) scavenger. The detailed experiment processes were similar to the photocatalytic activity experiments.

3. Results and Discussion

Figure 2 depicts scanning electron microscope (SEM) images of the as-prepared materials. A well-distributed micro-sphere structure (~5 μm) with smooth surface for pure $CuBi_2O_4$ is shown in Figure 2a. The transition material of $CuBi_2O_4$@C, from Figure 2b, shows increased size and relatively rough surface compared with pure $CuBi_2O_4$. Moreover, some dispersed carbon microspheres exist as well. In the formation process of $CuBi_2O_4/\beta$-Bi_2O_3, the control of temperature is an important step. As shown from Figure 2c, the products exhibit a chain-connected spherical structure when the temperature is at 400 °C, and the connection matter is the incompletely burned carbon. That is because the complete combustion temperature of carbon is higher than 500 °C [29]. Therefore, the composition of calcined products just contain $CuBi_2O_4$ and β-Bi_2O_3 when the temperatures are at 600 °C and 800 °C. But the rising of calcination temperature will destroy sphere-structural $CuBi_2O_4$, which can be seen from the SEM images of Figure 2d,e.

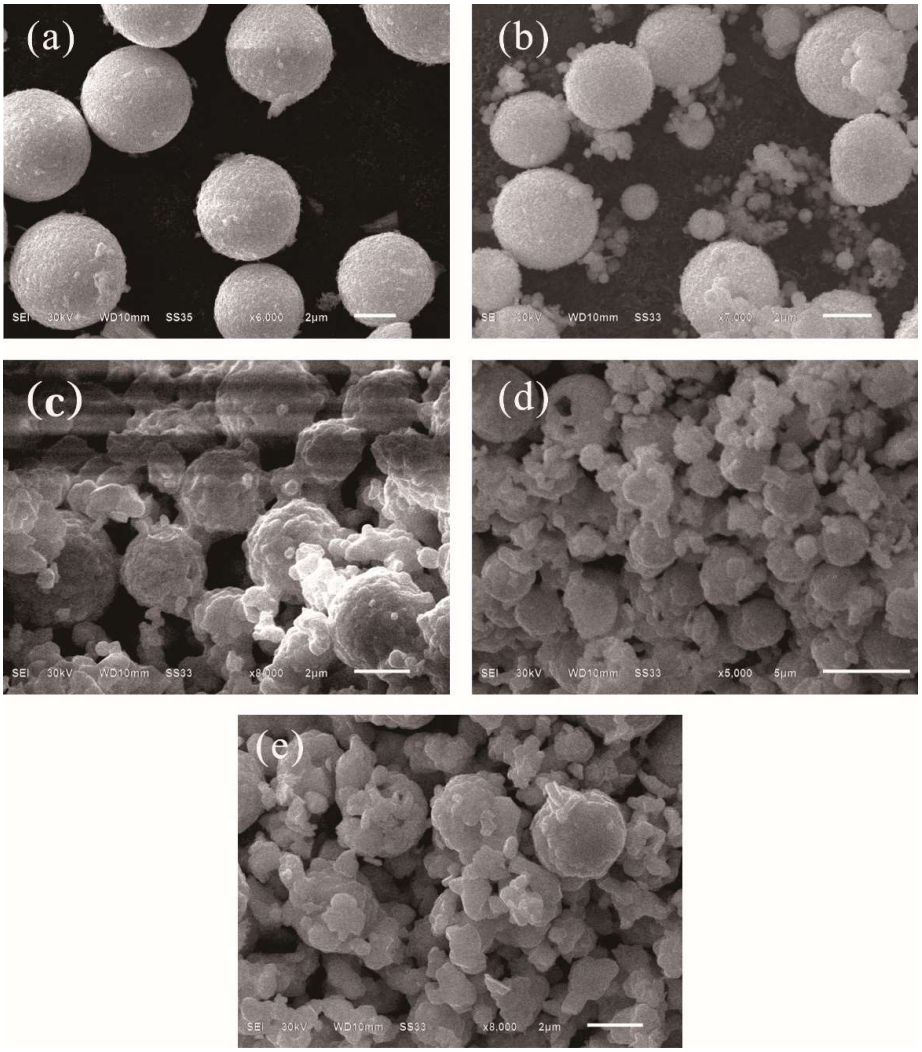

Figure 2. Scanning electron microscope (SEM) images of (**a**) $CuBi_2O_4$; (**b**) $CuBi_2O_4$@C; (**c**) $CuBi_2O_4/\beta$-Bi_2O_3 (1:2.25, 400 °C); (**d**) $CuBi_2O_4/\beta$-Bi_2O_3 (1:2.25, 600 °C); (**e**) $CuBi_2O_4/\beta$-Bi_2O_3 (1:2.25, 800 °C).

The purity and crystallinity of $CuBi_2O_4$ and $CuBi_2O_4/\beta$-Bi_2O_3 calcined at 600 °C were examined with XRD, as depicted in Figure 3. From the XRD pattern of $CuBi_2O_4$, the diffraction peaks can be perfectly indexed to the phase of $CuBi_2O_4$ (JCPDS No. 84-1969) [30]. In the XRD pattern of $CuBi_2O_4/\beta$-Bi_2O_3 (600 °C), except for the peaks indicating $CuBi_2O_4$, the diffraction peaks located at the 2θ values of 27.66°, 32.86°, 46.32°, 55.44°, and 57.86°, can be indexed to the (201), (220), (222), (421), and (402) crystalline planes of tetragonal β-Bi_2O_3 (JCPDS No. 27-0050) [22,25]. Moreover, there are no obvious carbon peaks from the XRD pattern of $CuBi_2O_4/\beta$-Bi_2O_3 (600 °C), indicating the complete combustion of carbon in this calcination temperature [29].

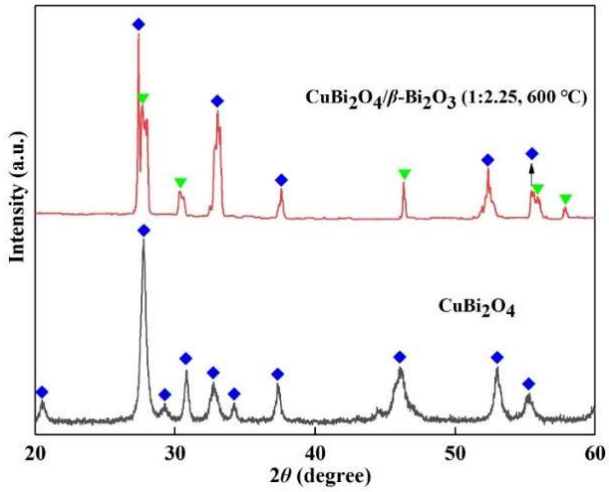

Figure 3. X-ray diffraction (XRD) patterns of $CuBi_2O_4$ and $CuBi_2O_4/\beta$-Bi_2O_3 (1:2.25, 600 °C).

The UV-Vis absorption spectrum of $CuBi_2O_4$, β-Bi_2O_3 (600 °C) and $CuBi_2O_4/\beta$-Bi_2O_3 (600 °C) are displayed in Figure 4a. Both of the materials exhibit strong absorbance in the UV and visible light regions, and the maximum absorption boundary of $CuBi_2O_4$, β-Bi_2O_3 (600 °C) and $CuBi_2O_4/\beta$-Bi_2O_3 (600 °C) appear at approximately 800 nm, 500 nm and 725 nm, respectively. The band gap energy (E_g) of $CuBi_2O_4$ and β-Bi_2O_3 (600 °C) can be determined with the classic Tauc approach by using the following equation [31]: $\alpha hv = A(hv - E_g)^{n/2}$, where α, h, v, E_g and A are the absorption coefficient, the Planck constant, the light frequency, the band gap energy, and a constant, respectively. In the equation, n is a number characteristic of the charge transition in a semiconductor, and n = 1 for a direct transition while n = 4 for an indirect transition [31]. As for $CuBi_2O_4$ and β-Bi_2O_3 (600 °C), n = 4 [32,33]. Therefore, their band gap energy could be elicited from the plot of light energy $(\alpha hv)^2$ versus energy (hv), shown in Figure 4b, which suggests that the band gap energy of $CuBi_2O_4$ and β-Bi_2O_3 (600 °C) are 1.72 eV and 2.70 eV, respectively, which are very close to previous literature [33–35]. In addition, the valence band (VB) and conduction band (CB) edge position of the semiconductors can be estimated according to the following empirical equation:

$$E_{VB} = X - E^c + 0.5E_g \quad (1)$$

$$E_{CB} = E_{VB} - E_g \quad (2)$$

where E_{VB} and E_{CB} are the valence band (VB) and conduction band (CB) edge potentials, respectively; X is the electronegativity of the absolute electronegativity of the constituent atoms, that is 4.59 eV for $CuBi_2O_4$ and 6.24 eV for β-Bi_2O_3 [25,33]; E^c is the energy of free electrons on the hydrogen scale (approximately 4.5 eV) [31]. Consequently, the E_{VB} and E_{CB} positions of $CuBi_2O_4$ are estimated to be 0.95 and −0.77 eV/NHE; the E_{VB} and E_{CB} positions of β-Bi_2O_3 (600 °C) are estimated to be 3.09 and 0.39 eV/NHE.

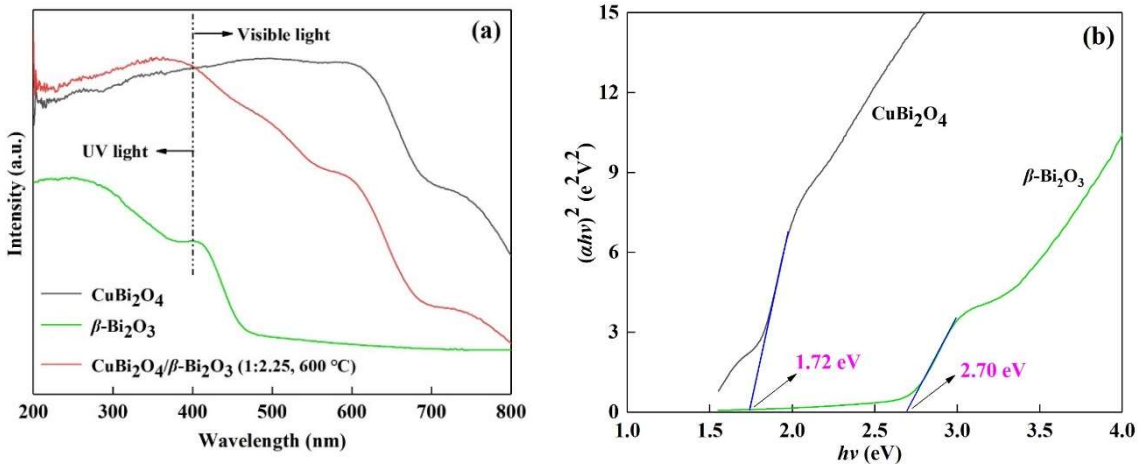

Figure 4. (**a**) Ultraviolet-visible (UV-Vis) diffuse reflectance spectra of $CuBi_2O_4$ and $CuBi_2O_4/\beta$-Bi_2O_3 (1:2.25, 600 °C); (**b**) band gap energy (E_g) of $CuBi_2O_4$ and $CuBi_2O_4/\beta$-Bi_2O_3 (1:2.25, 600 °C) derived from the plots of $(\alpha h\nu)^2$ versus energy ($h\nu$).

The degradation of DS in different photocatalytic systems was evaluated under visible light irradiation, and the results are described inFigure 5. It can be seen from Figure 5a, the degradation efficiency of DS in the blank irradiation system is 38.21% in 240 min reaction while the degradation efficiency of DS is 44.48% and 65.85% with the addition of pure β-Bi_2O_3 and $CuBi_2O_4$. As for the system of mechanically mixed $CuBi_2O_4$ and β-Bi_2O_3 with the mass ratio of 1:2.25, 70.11% of DS can be degraded in the same condition. Figure 5c shows the photodegradation efficiency of DS in the system of composites $CuBi_2O_4/\beta$-Bi_2O_3 with different mass ratios. The adsorption capacity of composites to DS is less than 10%, suggesting the removal of DS is closely related to photodegradation and photocatalysis. The degradation efficiency of DS is enhanced with increasing β-Bi_2O_3 in the composite as the mass ratio of $CuBi_2O_4$ and β-Bi_2O_3 changes from 1:0.5 to 1:2.25, but will decrease with a further increase of the content of β-Bi_2O_3, i.e., the mass ratio of 1:4. Figure 5e shows the degradation efficiency of DS using $CuBi_2O_4/\beta$-Bi_2O_3 calcined at different temperatures. It can be seen that the degradation efficiencies of DS are 84.37%, 92.17% and 76.80%, respectively, and the composites calcined at 400 °C, 600 °C and 800 °C. Figure 5b,d,f describe the degradation rate curves of DS in different photocatalytic systems which derive from the $\ln(C_0/C)$ versus irradiation time and the values of degradation rates are listed in Table 1. The maximum degradation rate of DS can be obtained in the system of composite $CuBi_2O_4/\beta$-Bi_2O_3 with the mass ratio of 1:2.25 and the calcination temperature of 600 °C, which is 0.0099 min^{-1}.

Table 1. Kinetic analysis of DS degradation in different photocatalyst systems.

Photocatalytic System	K_{app} (min^{-1})	R^2
Blank irradiation	0.0027	0.92
β-Bi_2O_3	0.0030	0.90
$CuBi_2O_4$	0.0040	0.94
Mechanically mixed with $CuBi_2O_4$ and β-Bi_2O_3	00048	0.94
$CuBi_2O_4/\beta$-Bi_2O_3 (1:0.5, 600 °C)	0.0055	0.92
$CuBi_2O_4/\beta$-Bi_2O_3 (1:1, 600 °C)	0.0076	0.91
$CuBi_2O_4/\beta$-Bi_2O_3 (1:2.25, 600 °C)	0.0099	0.90
$CuBi_2O_4/\beta$-Bi_2O_3 (1:4, 600 °C)	0.0059	0.96
$CuBi_2O_4/\beta$-Bi_2O_3 (1:2.25, 400 °C)	0.0065	0.95
$CuBi_2O_4/\beta$-Bi_2O_3 (1:2.25, 800 °C)	0.0060	0.95

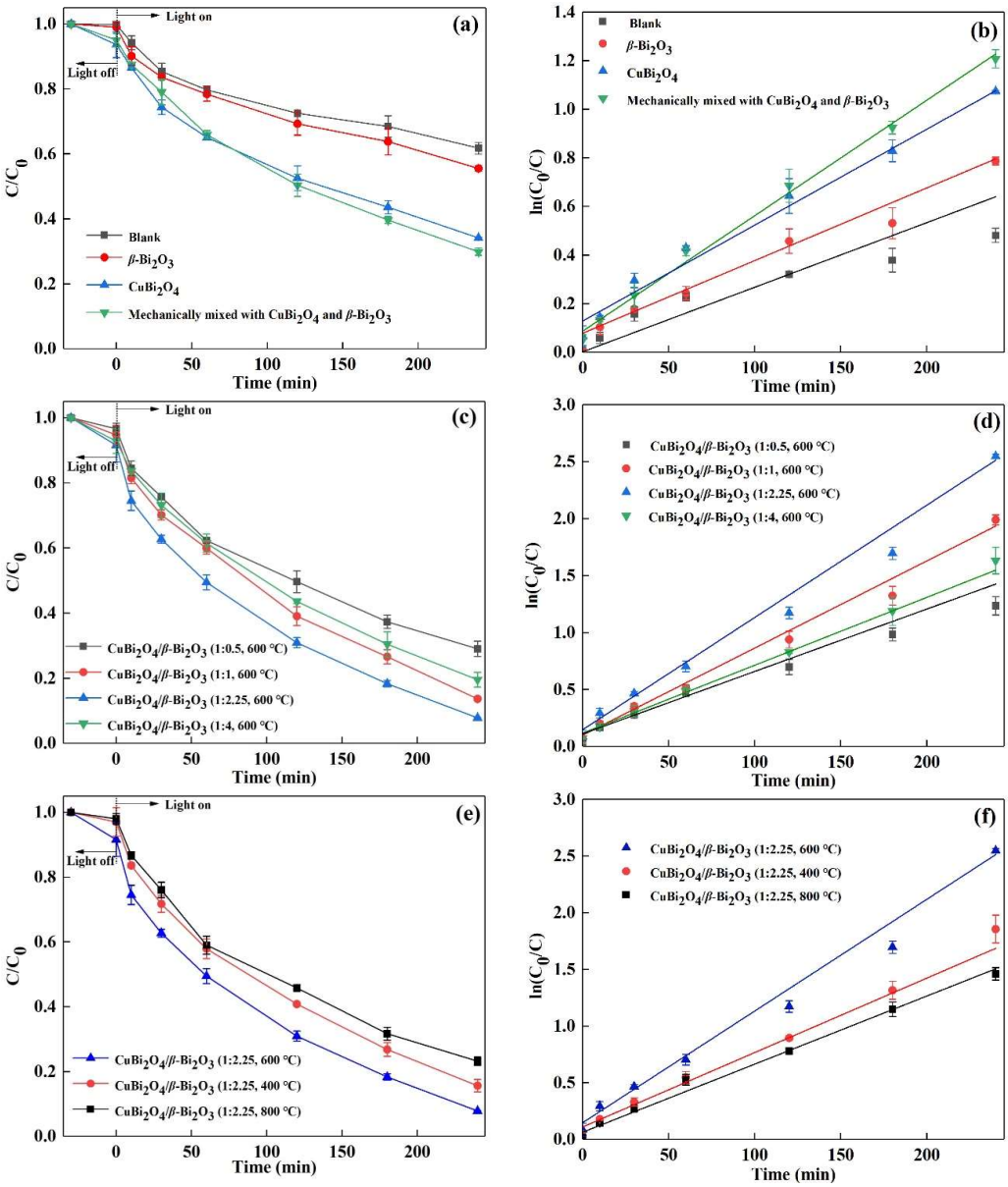

Figure 5. Diclofenac sodium (DS) degradation efficiency in the photocatalytic system of (**a**) blank irradiation, $CuBi_2O_4$, β-Bi_2O_3 and $CuBi_2O_4$ + β-Bi_2O_3; (**c**) $CuBi_2O_4/\beta$-Bi_2O_3 with different mass ratios; (**e**) $CuBi_2O_4/\beta$-Bi_2O_3 with different calcination temperatures; (**b**,**d**,**f**) plots of $\ln(C_0/C)$ versus irradiation time over different photocatalytic systems.

To further evaluate the degradation efficiency of DS in the as-prepared catalyst's system, the removal efficiencies of Total Organic Carbon (TOC) are also explored and the results are shown in Figure 6. In the blank irradiation system, only 18.01% of TOC can be removed. And in the pure β-Bi_2O_3 and $CuBi_2O_4$ photocatalytic systems, the TOC removal efficiencies are 22.52% and 30.59%, respectively. When $CuBi_2O_4$ and β-Bi_2O_3 with the mass ratio of 1:2.25 are mechanically mixed to add into the system, 35.96% of TOC are removed. But for the composites $CuBi_2O_4/\beta$-Bi_2O_3 with different mass ratios calcinated at various temperatures, the removal efficiencies of TOC can be greatly improved, and the maximum value reaches 57.37%, which is achieved in the photocatalytic system of $CuBi_2O_4/\beta$-Bi_2O_3 with the mass ratio of 1:2.25 and the calcination temperature of 600 °C.

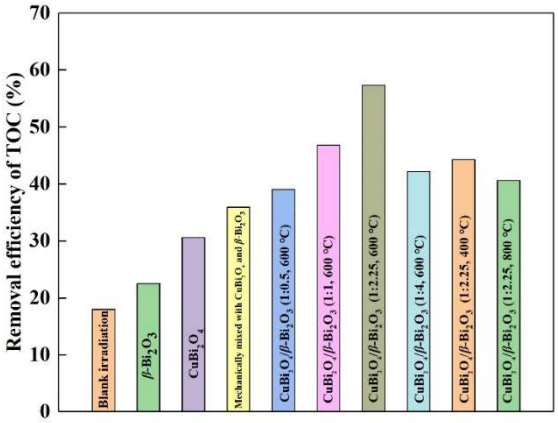

Figure 6. Total Organic Carbon (TOC) removal efficiency of the DS photodegradation solutions in different photocatalytic systems.

Figure 7a describes the photodegradation efficiency of DS under different recycling runs using $CuBi_2O_4/\beta$-Bi_2O_3 (1:2.25, 600 °C) as the catalyst. When the catalyst was repeated for seven times, the degradation efficiency of DS is 82.95%. Figure 7b shows the degradation rate curves of DS over $CuBi_2O_4/\beta$-Bi_2O_3 (1:2.25, 600 °C) under different recycling runs, and the values of rate constants are described in the illustration. It can be seen that the degradation rate of DS decreases from 0.0099 min^{-1} to 0.0071 min^{-1} after the seventh recycle. To further understand the photocatalytic stability of the as-prepared $CuBi_2O_4/\beta$-Bi_2O_3, XRD and Bi 4f XPS spectrums of the recycled composites are conducted seven times and the results are shown in Figure 8. Compared with the XRD spectra of the fresh and reused $CuBi_2O_4/\beta$-Bi_2O_3 in Figure 8a, there are no obvious changes for the main peaks. But from the Figure 8b, a new peak occur in the composite after recycling expect for the two main peaks existing in both of the two samples. According to reports, the main 4f 7/2 peak at 158.32 eV for a fresh sample and 158.30 eV for a reused sample, and the other main 4f 5/2 peak at 163.60 eV for a fresh sample and 163.49 eV for a reused sample, correspond to the Bi^{3+} oxidation state [36,37], which are in accordance to the presence of either $CuBi_2O_4$ or β-Bi_2O_3 phases. The extra peak at 156.63 eV in the reused sample is ascribed to Bi metal [38], indicating that some Bi^{3+} in the substance was reduced to be Bi metal after the reaction.

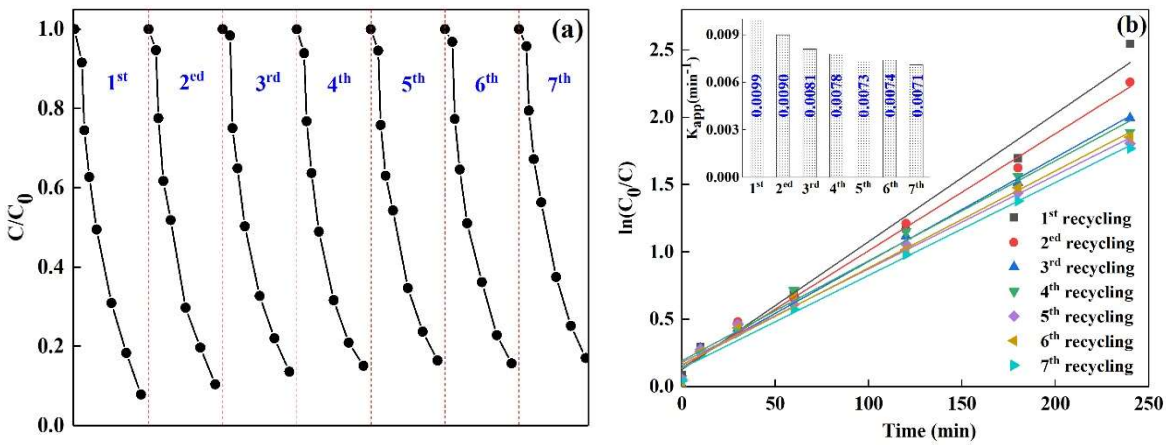

Figure 7. (**a**) Photodegradation efficiency of DS; (**b**) plots of $\ln(C_0/C)$ versus irradiation time over $CuBi_2O_4/\beta$-Bi_2O_3 (1:2.25, 600 °C) under different recycling runs. The illustration in (**b**) shows the degradation rate constants of DS under different recycling runs.

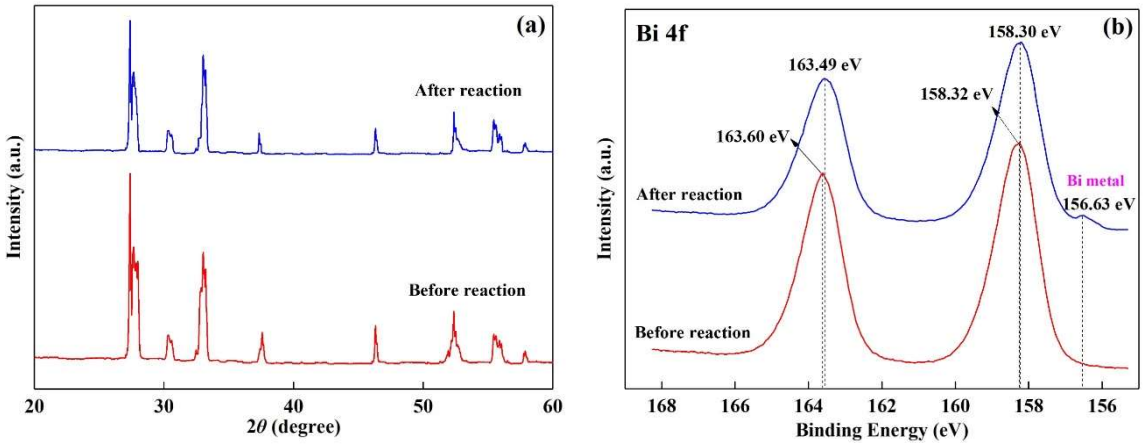

Figure 8. (**a**) XRD pattern; (**b**) Bi 4f X-ray photoelectron spectrum (XPS) of the composite catalyst $CuBi_2O_4/\beta$-Bi_2O_3 (1:2.25, 600 °C) before and after reaction for seventh times.

Moreover, the free radical capture experiments used to investigate the active species involved in the DS degradation with the $CuBi_2O_4/\beta$-Bi_2O_3 (1:2.25, 600 °C) photocatalyst are explored and the results are shown in Figure 9. The degradation efficiency of DS decreases to 41.74% when 1 mM EDTA-Na_2 was added, and the DS degradation was completely inhibited with the addition of 2 mM EDTA-Na_2. But the degradation efficiency of DS decreases to 54.98% and 27.82% when 2 mM *t*-BuOH or BZQ was added, respectively. The results suggest that the enhanced photocatalytic activity of $CuBi_2O_4/\beta$-Bi_2O_3 is closely related to $OH^{\bullet}$, h^+ and $O_2^{\bullet-}$, and the contribution order is $h^+ > O_2^{\bullet-} > OH^{\bullet}$.

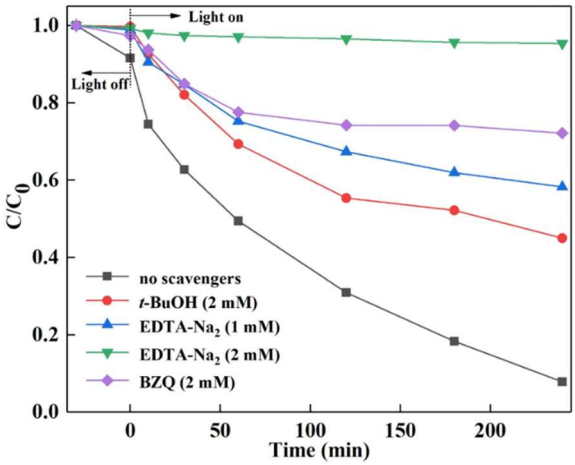

Figure 9. Photodegradation efficiency of DS under different scavengers in the system of $CuBi_2O_4/\beta$-Bi_2O_3 (1:2.25, 600 °C).

As for the photocatalytic mechanisms of a semiconductor–semiconductor composite catalyst, the heterojunction energy band theory and Z-scheme theory were of concern [8]. Based on the analysis above, a possible Z-scheme photocatalytic mechanism was put forward to explain the enhanced photocatalytic activity of the $CuBi_2O_4/\beta$-Bi_2O_3 composite, which is illustrated in Figure 10. That is, both $CuBi_2O_4$ and β-Bi_2O_3 could generate the photoinduced electron-hole pairs under visible-light illumination owing to their good light absorption abilities. Then, the formed Bi metal becomes the recombination center of the photogenerated electron from CB of β-Bi_2O_3 and the holes from the VB of the $CuBi_2O_4$ in the photocatalytic reaction process, leading to the improved charge separation. Besides, the dissolved O_2 in the solution can be captured by the photogenerated electrons in the CB of $CuBi_2O_4$ to form $O_2^{\bullet-}$ due to the more negative CB level of $CuBi_2O_4$ than the potential of $O_2/O_2^{\bullet-}$

($E(O_2/O_2^{\bullet-})$ = 0.13 eV (vs. NHE) [39]; while the photogenerated holes in the VB of β-Bi_2O_3 can lead the H_2O/OH^- to be oxidized to $OH^\bullet$ for the higher energy of holes in the VB of β-Bi_2O_3 than the potential of $OH^-/OH^\bullet$ $E(OH^-/OH^\bullet)$ = 1.99 eV (vs. NHE) [39]. Subsequently, the holes in the VB of β-Bi_2O_3, the formed $OH^\bullet$ and $O_2^{\bullet-}$ participate in the DS photodegradation.

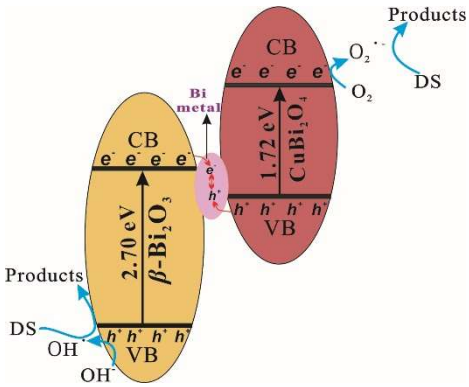

Figure 10. Supposed photocatalytic mechanism of $CuBi_2O_4/\beta$-Bi_2O_3 by the Z-scheme theory.

4. Conclusions

A combined hydrothermal and temperature-programmed method was employed to synthesize the $CuBi_2O_4/\beta$-Bi_2O_3 composite photocatalysts. The properties of the as-prepared materials were systematically characterized by SEM, XRD, XPS and UV-Vis. Moreover, the composites exhibit enhanced photocatalytic performance toward DS degradation under visible light irradiation, and the optimal photodegradation efficiency of DS is achieved in the catalytic system of $CuBi_2O_4/\beta$-Bi_2O_3 with the mass ratio of 1:2.25 and the calcination temperature of 600 °C. Besides, the active species in the $CuBi_2O_4/\beta$-Bi_2O_3 photocatalytic system were discussed through the free radical capture experiments, and the photocatalytic mechanism of $CuBi_2O_4/\beta$-Bi_2O_3 was also put forward.

Author Contributions: X.C. (Xiaojuan Chen) designed and performed the experiments, and drafted the manuscript. N.L. and R.Z. provided guidance for the general idea of the thesis. S.L., C.Y., W.X., S.X. and X.C. (Xin Chen) carried out the sample preparations, part of the material characterization analysis, and data collection. All authors read and approved the final manuscript.

Funding: This research was funded by the National Natural Science Foundation of China [grant number 51708116], the Science and Technology Planning Project of Guangdong Province, China [grant number 2017B030314175], and the Scientific Research Foundation for High-level Talents of Foshan University [grant number gg07014].

Acknowledgments: This work has been financially supported by the National Natural Science Foundation of China (No. 51708116), the Science and Technology Planning Project of Guangdong Province, China (No. 2017B030314175), and the Scientific Research Foundation for High-level Talents of Foshan University (No. gg07014).

Conflicts of Interest: The authors declare no conflict of interest.

References

1. Song, S.; Su, Y.; Adeleye, A.S.; Zhang, Y.; Zhou, X. Optimal design and characterization of sulfide-modified nanoscale zerovalent iron for diclofenac removal. *Appl. Catal. B Environ.* **2017**, *201*, 211–220. [CrossRef]
2. Thiruppathi, M.; Kumar, P.S.; Devendran, P.; Ramalingan, C.; Swaminathan, M.; Nagarajan, E.R. Ce@TiO_2 nanocomposites: An efficient, stable and affordable photocatalyst for the photodegradation of diclofenac sodium. *J. Alloys Compd.* **2017**, *735*, 728–734. [CrossRef]
3. Espino-Estévez, M.R.; Fernández-Rodríguez, C.; González-Díaz, O.M.; Araña, J.; Espinós, J.P.; Ortega-Méndez, J.A.; Doña-Rodríguez, J.M. Effect of TiO_2-Pd and TiO_2-Ag on the photocatalytic oxidation of diclofenac, isoproturon and phenol. *Chem. Eng. J.* **2016**, *298*, 82–95. [CrossRef]

4. Chen, X.J.; Li, N.; Xu, S.; Wang, H.L.; Cai, Y.M. Study on the visible-light photocatalytic performance and degradation mechanism of diclofenac sodium under the system of hetero-structural $CuBi_2O_4/Ag_3PO_4$ with H_2O_2. *Materials* **2018**, *11*, 511. [CrossRef] [PubMed]
5. Liao, C.H.; Huang, C.W.; Wu, J.C.S. Hydrogen production from semiconductor-based photocatalysis via water splitting. *Catalysts* **2012**, *2*, 490–516. [CrossRef]
6. Natarajan, T.S.; Thampi, K.R.; Tayade, R.J. Visible light driven redox-mediator-free dual semiconductor photocatalytic systems for pollutant degradation and the ambiguity in applying Z-scheme concept. *Appl. Catal. B Environ.* **2018**, *227*, 296–311. [CrossRef]
7. Wang, L.; Cai, M.; Sun, W.; He, L.; Zhang, X. Promoting charge separation in semiconductor nanocrystal superstructures for enhanced photocatalytic activity. *Adv. Mater. Interfaces* **2018**, *1701694*. [CrossRef]
8. Zhou, P.; Yu, J.; Jaroniec, M. All-solid-state Z-scheme photocatalytic systems. *Adv. Mater.* **2014**, *26*, 4920–4935. [CrossRef] [PubMed]
9. Bianchi, C.L.; Pirola, C.; Galli, F.; Stucchi, M.; Morandi, S.; Cerrato, G.; Capucci, V. Nano and micro-TiO_2 for the photodegradation of ethanol: Experimental data and kinetic modelling. *RSC Adv.* **2015**, *5*, 53419–53425. [CrossRef]
10. Ochiai, T.; Fujishima, A. Photoelectrochemical properties of TiO_2 photocatalyst and its applications for environmental purification. *J. Photochem. Photobiol. C Photochem. Rev.* **2012**, *13*, 247–262. [CrossRef]
11. Kumar, S.G.; Devi, L.G. Review on modified TiO_2 photocatalysis under UV/visible light: Selected results and related mechanisms on interfacial charge carrier transfer dynamics. *J. Phys. Chem. A* **2011**, *115*, 13211–13241. [CrossRef] [PubMed]
12. Pelaez, M.; Nolan, N.T.; Pillai, S.C.; Seery, M.K.; Falaras, P.; Kontos, A.G.; Dunlop, P.S.M.; Hamilton, J.W.J.; Byrne, J.A.; O'Shea, K. A review on the visible light active titanium dioxide photocatalysts for environmental applications. *Appl. Catal. B Environ.* **2012**, *125*, 331–349. [CrossRef]
13. Wang, Y.; Wang, Q.; Zhan, X.; Wang, F.; Safdar, M.; He, J. Visible light driven type II heterostructures and their enhanced photocatalysis properties: A review. *Nanoscale* **2013**, *5*, 8326–8339. [CrossRef] [PubMed]
14. Moniz, S.J.A.; Shevlin, S.A.; Martin, D.J.; Guo, Z.X.; Tang, J. Visible-light driven heterojunction photocatalysts for water splitting-a critical review. *Energy Environ. Sci.* **2015**, *8*, 731–759. [CrossRef]
15. Dong, S.; Feng, J.; Fan, M.; Pi, Y.; Hu, L.; Han, X.; Liu, M.; Sun, J.; Sun, J. Recent developments in heterogeneous photocatalytic water treatment using visible light-responsive photocatalysts: A review. *RSC Adv.* **2015**, *5*, 14610–14630. [CrossRef]
16. Chen, X.J.; Dai, Y.Z.; Guo, J. Hydrothermal synthesis of well-distributed spherical $CuBi_2O_4$ with enhanced photocatalytic activity under visible light irradiation. *Mater. Lett.* **2015**, *161*, 251–254. [CrossRef]
17. Guo, F.; Shi, W.; Wang, H.; Han, M.; Guan, W.; Huang, H.; Liu, Y.; Kang, Z. Study on highly enhanced photocatalytic tetracycline degradation of type II $AgI/CuBi_2O_4$ and Z-scheme $AgBr/CuBi_2O_4$ heterojunction photocatalysts. *J. Hazard. Mater.* **2018**, *349*, 111–118. [CrossRef] [PubMed]
18. Oh, W.D.; Lua, S.K.; Dong, Z.; Lim, T.T. Rational design of hierarchically-structured $CuBi_2O_4$ composites by deliberate manipulation of the nucleation and growth kinetics of $CuBi_2O_4$ for environmental applications. *Nanoscale* **2015**, *8*, 2046–2054. [CrossRef] [PubMed]
19. Hossain, M.K.; Samu, G.F.; Gandha, K.; Santhanagopalan, S.; Liu, J.P.; Janáky, C.; Rajeshwar, K. Solution combustion synthesis, characterization, and photocatalytic activity of $CuBi_2O_4$ and its nanocomposites with CuO and α-Bi_2O_3. *J. Phys. Chem. C* **2017**, *121*, 8252–8261. [CrossRef]
20. Wang, Y.; Li, F.; Xue, T.; Liu, C.; Yuan, D.; Qi, F.; Xu, B. Heterogeneous activation of peroxymonosulfate by hierarchical $CuBi_2O_4$ to generate reactive oxygen species for refractory organic compounds degradation: Morphology and surface chemistry derived reaction and its mechanism. *Environ. Sci. Pollut. Res.* **2018**, *25*, 4419–4434. [CrossRef] [PubMed]
21. Muñozbatista, M.J.; Kubacka, A.; Fontellescarceller, O.; Tudela, D.; Fernandezgarcia, M. Surface CuO, Bi_2O_3, and CeO_2 species supported in TiO_2-anatase: Study of interface effects in toluene photodegradation quantum efficiency. *ACS Appl. Mater. Interfaces* **2016**, *8*, 13934–13945. [CrossRef] [PubMed]
22. Chen, Y.; Zhang, Y.; Luo, L.; Shi, Y.; Wang, S.; Li, L.; Long, Y.; Jiang, F. A novel templated synthesis of C/N-doped β-Bi_2O_3 nanosheets for synergistic rapid removal of 17α-ethynylestradiol by adsorption and photocatalytic degradation. *Ceram. Int.* **2018**, *44*, 2178–2185. [CrossRef]

23. Gadhi, T.A.; Hernández, S.; Castellino, M.; Jagdale, P.; Husak, T.; Hernández-Gordillo, A.; Tagliaferro, A.; Russo, N. Insights on the role of β-Bi_2O_3/$Bi_5O_7NO_3$ heterostructures synthesized by a scalable solid-state method for the sunlight-driven photocatalytic degradation of dyes. *Catal. Today* **2018**. [CrossRef]
24. Hwang, H.; Shin, J.; Lee, K.Y.; Choi, W. Facile one-pot transformation using structure-guided combustion waves of micro-nanostructured β-Bi_2O_3 to α-Bi_2O_3@C and analysis of electrochemical capacitance. *Appl. Surf. Sci.* **2018**, *428*, 422–431. [CrossRef]
25. Chang, C.; Yang, H.C.; Gao, N.; Lu, S.Y. Core/shell p-BiOI/n-β-Bi_2O_3 heterojunction array with significantly enhanced photoelectrochemical water splitting efficiency. *J. Alloys Compd.* **2018**, *738*, 138–144. [CrossRef]
26. Hong, Y.; Li, C.; Yin, B.; Li, D.; Zhang, Z.; Mao, B.; Fan, W.; Gu, W.; Shi, W. Promoting visible-light-induced photocatalytic degradation of tetracycline by an efficient and stable beta-Bi_2O_3@g-C_3N_4 core/shell nanocomposite. *Chem. Eng. J.* **2018**, *338*, 137–146. [CrossRef]
27. Xiong, M.; Chen, L.; Yuan, Q.; He, J.; Luo, S.L.; Au, C.T.; Yin, S.F. Controlled synthesis of graphitic carbon nitride/beta bismuth oxide composite and its high visible-light photocatalytic activity. *Carbon* **2015**, *86*, 217–224. [CrossRef]
28. Cong, Y.; Wang, J.; Jin, H.; Xiao, F.; Qi, W.; Yun, J.; Yi, Z. Enhanced photoelectrocatalytic activity of a novel Bi_2O_3-$BiPO_4$ composite electrode for the Degradation of refractory pollutants under visible light irradiation. *Ind. Eng. Chem. Res.* **2016**, *55*, 1221–1228. [CrossRef]
29. Bazargan, A.; Yan, Y.; Hui, C.W.; Mckay, G. A Review: Synthesis of carbon-based nano and micro materials by high temperature and high pressure. *Ind. Eng. Chem. Res.* **2013**, *52*, 12689–12702. [CrossRef]
30. Berglund, S.P.; Abdi, F.F.; Bogdanoff, P.; Chemseddine, A.; Friedrich, D.; Krol, R.V.D. Comprehensive evaluation of $CuBi_2O_4$ as a photocathode material for photoelectrochemical water splitting. *Chem. Mater.* **2016**, *28*, 4231–4242. [CrossRef]
31. Chang, C.; Zhu, L.; Wang, S.; Chu, X.; Yue, L. Novel mesoporous graphite carbon nitride/BiOI heterojunction for enhancing photocatalytic performance under visible-light irradiation. *ACS Appl. Mater. Interfaces* **2014**, *6*, 5083–5093. [CrossRef] [PubMed]
32. Xiao, X.; Hu, R.; Liu, C.; Xing, C.; Qian, C.; Zuo, X.; Nan, J.; Wang, L. Facile large-scale synthesis of β-Bi_2O_3 nanospheres as a highly efficient photocatalyst for the degradation of acetaminophen under visible light irradiation. *Appl. Catal. B Environ.* **2013**, *140–141*, 433–443. [CrossRef]
33. Patil, R.; Kelkar, S.; Naphade, R.; Ogale, S. Low temperature grown $CuBi_2O_4$ with flower morphology and its composite with CuO nanosheets for photoelectrochemical water splitting. *J. Mater. Chem. A* **2014**, *2*, 3661–3668. [CrossRef]
34. Wang, Q.; Liu, E.; Zhang, C.; Huang, S.; Cong, Y.; Zhang, Y. Synthesis of $Cs_3PMo_{12}O_{40}$/Bi_2O_3 composite with highly enhanced photocatalytic activity under visible-light irradiation. *J. Colloid Interface Sci.* **2018**, *516*, 304–311. [CrossRef] [PubMed]
35. Li, Y.; Wang, J.; Yao, H.; Dang, L.; Li, Z. Chemical etching preparation of BiOI/Bi_2O_3 heterostructures with enhanced photocatalytic activities. *Catal. Commun.* **2011**, *12*, 660–664. [CrossRef]
36. Li, J.; Zhong, J.; He, X.; Huang, S.; Zeng, J.; He, J.; Shi, W. Enhanced photocatalytic activity of Fe_2O_3 decorated Bi_2O_3. *Appl. Surf. Sci.* **2013**, *284*, 527–532. [CrossRef]
37. Uchida, K.; Ayame, A. Dynamic XPS measurements on bismuth molybdate surfaces. *Surf. Sci.* **1996**, *357–358*, 170–175. [CrossRef]
38. Diez, E.; Monnereau, O.; Tortet, L.; Vacquier, G.; Llewellin, P.; Rouquerol, F. Synthesis of bismuth (III) oxide from oxalate: A study by controlled transformation rate thermal analysis (CRTA). *J. Optoelectron. Adv. Mater.* **2000**, *2*, 552–556.
39. Guo, J.; Ouyang, S.; Zhou, H.; Kako, T.; Ye, J. Ag_3PO_4/$In(OH)_3$ composite photocatalysts with adjustable surface-electric property for efficient photodegradation of organic dyes under simulated solar-light irradiation. *J. Phys. Chem. C* **2013**, *117*, 17716–17724. [CrossRef]

© 2018 by the authors. Licensee MDPI, Basel, Switzerland. This article is an open access article distributed under the terms and conditions of the Creative Commons Attribution (CC BY) license (http://creativecommons.org/licenses/by/4.0/).